

1-1-2010

Plasmonic Light-trapping and Quantum Efficiency Measurements on Nanocrystalline Silicon Solar Cells and Silicon-On-Insulator Devices

Eric A. Schiff

Syracuse University, easchiff@syr.edu

Hui Zhao

Syracuse University

Birol Ozturk

Syracuse University

Baojie Yan

United Solar Ovonic LLC

Jeff Yang

United Solar Ovonic LLC

Follow this and additional works at: <http://surface.syr.edu/phy>



Part of the [Physics Commons](#)

Repository Citation

“Plasmonic Light-trapping and Quantum Efficiency Measurements on Nanocrystalline Silicon Solar Cells and Silicon-On-Insulator Devices”, Hui Zhao, Birol Ozturk, E. A. Schiff, Baojie Yan, J. Yang and S. Guha, in *Amorphous and Polycrystalline Thin-Film Silicon Science and Technology* — 2010, edited by Q. Wang, B. Yan, S. Higashi, C.C. Tsai, A. Flewitt (Mater. Res. Soc. Symp. Proc. Volume 1245, Warrendale, Pennsylvania), pp. A03-02 – A03-07.

This Conference Document is brought to you for free and open access by the College of Arts and Sciences at SURFACE. It has been accepted for inclusion in Physics by an authorized administrator of SURFACE. For more information, please contact surface@syr.edu.

Plasmonic Light-trapping and Quantum Efficiency Measurements on Nanocrystalline Silicon Solar Cells and Silicon-On-Insulator Devices

Hui Zhao¹, Birol Ozturk¹, E. A. Schiff¹, Baojie Yan², J. Yang² and S. Guha²

¹Department of Physics, Syracuse University, Syracuse, New York 13244-1130, U.S.A.

²United Solar Ovonic LLC, Troy, Michigan 48084, U.S.A.

ABSTRACT

Quantum efficiency measurements in nanocrystalline silicon (nc-Si:H) solar cells deposited onto textured substrates indicate that these cells are close to the "stochastic light-trapping limit" proposed by Yablonoitch in the 1980s. An interesting alternative to texturing is "plasmonic" light-trapping based on non-textured cells and using an overlayer of metallic nanoparticles to produce light-trapping. While this type of light-trapping has not yet been demonstrated for nc-Si:H solar cells, significant photocurrent enhancements have been reported on silicon-on-insulator devices with similar optical properties to nc-Si:H. Here we report our measurements of quantum efficiencies in nc-Si:H solar cells and normalized photoconductance spectra in SOI photodetectors with and without silver nanoparticle layers. As was done previously, the silver nanoparticles were created by thermal annealing of evaporated silver thin films. We observed enhancement in the normalized photoconductance spectra of SOI photodetectors at longer wavelengths with the silver nanoparticles. For nc-Si:H solar cells, we have not yet observed significant improvement of the quantum efficiency with the addition of annealed silver films.

INTRODUCTION

Light trapping is essential in thin film solar cells due to the limited optical pathlength of photons at longer wavelengths. Their limited thickness does not allow complete light absorption at these wavelengths. Conventionally, both surfaces are textured in order to increase the scattering angles of the light from these interfaces that leads to stochastic light trapping. For a material with refractive index n , perfect texturing will enable as high as $4n^2$ times pathlength enhancement (about 50 for Si) as predicted by Yablonoitch [1].

Plasmonic light trapping is an emerging alternative to stochastic light trapping. A deep understanding of the plasmonic light trapping mechanism has not been presented yet, however experimental data shows that this light trapping scheme can lead to significant enhancements in semiconductor devices and solar cells. Stuart and Hall demonstrated a 20-fold photocurrent enhancement on silicon-on-insulator (SOI) photodetectors with the deposition of silver nanoparticles on the top silicon layer [2]. This experiment was reproduced by Pillai, *et al.* using SOI substrates with thicker top silicon layers [3], where they observed 18 times photocurrent enhancement at $\lambda = 1200$ nm. This group recently reported six times photocurrent enhancement on a 20 micron thick crystalline silicon solar cell [4]. Schaadt, *et al.* deposited colloidal gold nanoparticles on a silicon photodiode and observed up to 1.8 times photocurrent enhancement [5].

Here, we report our experimental results on the effects of silver nanoparticle films deposited onto the top conductive oxide layers of hydrogenated nanocrystalline silicon (nc-Si:H) solar cells. The silver films cause an overall loss in the external quantum efficiencies (QE) of solar cells. Experiments on SOI photodetectors with the same thickness of the active silicon layer

and similar silver nanoparticle films resulted in photocurrent enhancements at longer wavelengths. We present an analytical calculation of the effective nanoparticle polarizability for SOI top silicon layer and ITO layer of the solar cells. In addition, we used a discrete dipole approximation (DDA) method to calculate the re-radiation efficiency of different size nanoparticles. These calculations showed that the re-radiation is enhanced with increasing diameter and particles with diameters larger than 80 nm should be used in plasmonic efficiency enhancement experiments.

EXPERIMENT

The nc-Si:H solar cells were fabricated at United Solar Ovonic. The single junction cells had *nip* configuration and were deposited on stainless-steel substrates with a nominally specular Ag/ZnO (500 nm/130 nm thick) back-reflectors [6]. The intrinsic layer thickness was chosen to be 2.0 μm in order to match the silicon layer thickness of SOI substrates that we used in this study. The top-contact/anti-reflection layer on the nc-Si:H cells was a 70 nm thick indium-tin-oxide (ITO) film

Figure 1 shows the QE of the solar cell as-received, after addition of a silver layer and annealing (to create nanoparticles), and after annealing alone. Curve (a) represents the QE of the unprocessed solar cell; note the interference fringes visible at longer wavelengths. The decline in QE at shorter wavelengths is mainly due to absorption by the *p*-layer as well as by reduced anti-reflection coating efficiency. Two solar cells with the same QE spectra as depicted by curve (a) were annealed at 200°C for two hours. For one of the cells, the ITO layer was first covered with

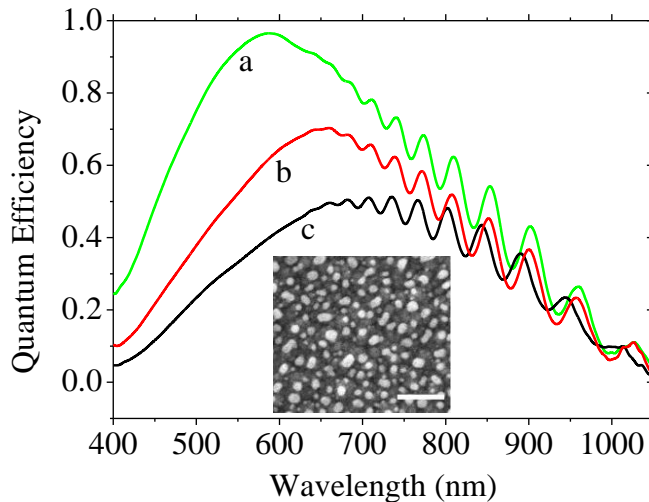


Figure 1. QEs of a nc-Si:H solar cell before and after deposition of annealed silver films; (a) as received (b) annealed without silver layer (c) with annealed silver film. Inset shows the scanning electron microscope (SEM) image of annealed silver films on top of ITO layer with 1 micron scale bar.

a 17 nm thick evaporated silver film [7]. Curve (b) shows the QE of the annealed solar cell without the silver layer; the anneal resulted in a significant overall reduction in the QE, which we believe is due to the degradation of the *p* layer. Curve (c) shows results for a cell with the silver layer. After annealing, silver nanoparticles formed on the surface of the ITO layer as shown in the inset of Figure 1. The reduction in the QE of the solar cell (curve c) with the nanoparticles was larger than for the annealed sample without silver. The larger reduction at shorter wavelengths in curve (c) is attributed to the lower re-radiation efficiency of the smaller size (<50nm) nanoparticles; this will be covered in detail in the discussion section. A blue-shift of the interference fringes was observed at longer wavelengths and will be discussed elsewhere [8].

We have also fabricated annealed silver films on SOI photodetectors. The SOI wafers were purchased from University Wafers, Inc.. The top silicon layer was 2 μm thick with 500 nm back oxide thickness. The annealed silver films were fabricated using the same method and parameters as for the nc-Si:H solar cells. The SEM image of the resulting silver nanoparticles is shown in the inset of Figure 2. Coplanar aluminum electrodes were thermally evaporated for lateral photocurrent measurements. An external quantum efficiency setup was used to measure the wavelength-dependent normalized photoconductance spectra $G_p(\lambda)/eF(\lambda)$, where G_p is the photoconductance due to the monochromator beam, e is the electronic charge, and F is the incident photon flux from the monochromator. The spectra without the silver particles showed moderate interference fringes. The addition of silver nanoparticles caused a reduction at shorter wavelengths ($\lambda < 520$ nm) and enhancement at longer wavelengths ($\lambda > 670$ nm).

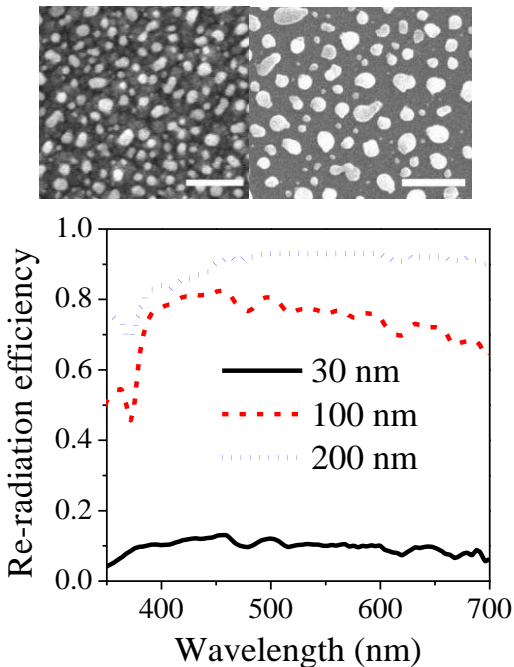


Figure 3. SEM images of the annealed silver films on ITO (top left) and on silicon (top right) surfaces. Scale bars denote 1 micron. DDA simulation results of the re-radiation efficiency dependence on the particle size (bottom).

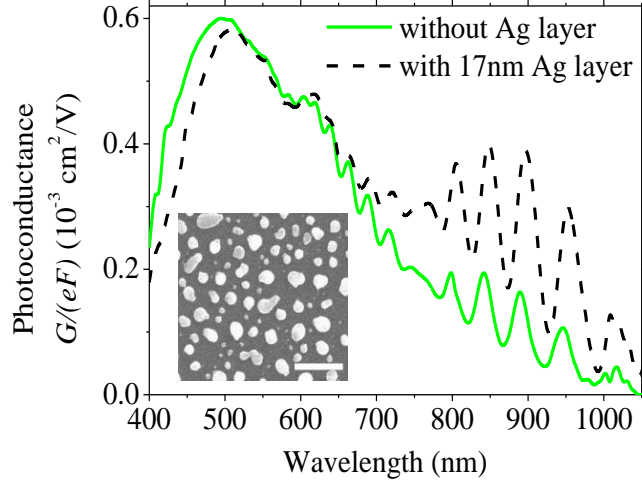


Figure 2. Normalized photoconductance spectra of the SOI photodetector with and without annealed silver film. Inset shows the SEM image of annealed silver films on the silicon layer with 1 micron scale bar. The spectra without the silver particles showed moderate interference fringes. The addition of silver nanoparticles caused a reduction at shorter wavelengths ($\lambda < 520$ nm) and enhancement at longer wavelengths ($\lambda > 670$ nm). A red-shift of the interference fringes is observed at longer wavelengths. These results are similar to our previous experiments where the Ag films were deposited onto 30 nm LiF spacer layers [8].

DISCUSSION

The annealed silver films lead to different results on nc-Si:H solar cells and SOI photodetectors. The main difference between the two structures is the additional 70 nm ITO top electrode layer on the nc-Si:H solar cells. The average nanoparticle diameter in the annealed silver films varied on these substrates (Figure 3). The particles on the silicon surface have larger average diameters (~ 200 nm) compared to particles on the ITO surface (~ 100 nm), presumably due to different "wetting" properties of these surfaces for Ag. There is also a larger density of smaller diameter (< 50 nm) silver nanoparticles on the ITO surface compared to the SOI surface. These smaller nanoparticles absorb a larger fraction of the incident field and turn into

heat energy, thus they have less re-radiation efficiency as will be shown subsequently.

We have performed numerical calculations of the re-radiation efficiency for different size silver nanoparticles using a discrete-dipole approximation (DDA) computer code DDSCAT 7.0 developed by Draine and Flatau [9]. Silver nanoparticles were modeled as oblate spheroids in air with dimensions $r_{maj}=2 r_{min}=30, 100, \text{ and } 200 \text{ nm}$, where r_{maj} and r_{min} are radii of the major and minor axes, respectively. The dielectric constants for silver were taken from literature [10]. Simulation results are shown in the lower panel of Figure 3. The re-radiation efficiency of the smaller diameter nanoparticles (30 nm) is below 20 % and it is over 70 % for larger diameter nanoparticles (100 nm and 200 nm). These results are in good agreement with the previous work [2] and they suggest that the smaller nanoparticles on the ITO layers of the solar cells are causing plasmonic extinction of the incident field; part of the energy is lost as heat before it reaches the active silicon layer. The reduction in the QE spectra of the solar cells with the addition of annealed silver films shown in Figure 1 was partly attributed to this effect.

We now turn to the effect of the substrate on the nanoparticle polarizability α_{eff} at optical frequencies. The effects of embedding a nanoparticle into a dielectric are well established [11], and the corresponding formulae for the polarizability α_0 of a spheroidal nanoparticle are given in the appendix. In our experiments, the silver nanoparticles were located near the interface of two materials with different refractive indices instead of being surrounded by a single medium. The effective polarizability of a spherical nanoparticle that is placed near the interface of two dielectric materials is given by [12]:

$$\alpha_{eff} = \alpha_0 \frac{1 + \beta}{1 - \beta \frac{\alpha_0}{16\pi(r+d)^3}}, \quad \beta = \frac{\epsilon_s - \epsilon_m}{\epsilon_s + \epsilon_m}, \quad (1)$$

where r is the radius of the sphere, d is the distance from the bottom edge of the particle to the interface, ϵ_s is the dielectric constant of the substrate material, and ϵ_m is the dielectric constant of the medium surrounding the nanoparticle. Following Protsenko and O'Reilly [13], we have utilized this analysis to calculate the effective polarizabilities for an oblate spheroidal silver nanoparticle near to an air/silicon and to an air/ITO interface; we identify r in eq. (1) as the semiminor axis r_{min} of the spheroid, and use the appropriately modified formulae for α_0 . The wavelength dependent dielectric constant values for ITO and for Si were taken from the literature [14,15].

The magnitude of the effective polarizability of the spheroid silver nanoparticle on ITO and silicon layer is shown in Figure 4. The silver nanoparticles were modeled as oblate

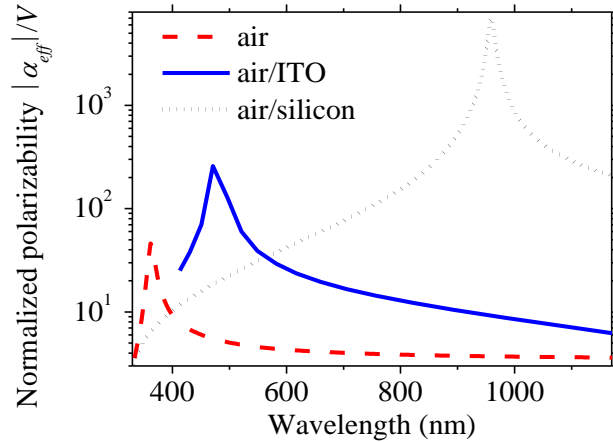


Figure 4. Calculated magnitude of the complex effective polarizability per unit volume for an oblate spheroidal silver nanoparticle (100 nm x 50 nm) in air, and 1 nm above ITO and silicon.

spheroids ($r_{maj} = 2 r_{min} = 100$ nm and $d = 1$ nm) with the major axes parallel to the substrate surface. This calculation shows that the plasmon frequency of the nanoparticle slightly red-shifts and its polarizability magnitude increased when placed on ITO layer. A large red-shift of the plasmon frequency and more than 150-fold increase in the polarizability magnitude is apparent when the nanoparticle is placed on a silicon surface compared to air.

The particle absorption and scattering cross sections are given by [16]:

$$c_{abs} = k \operatorname{Im}\{\alpha\} \quad c_{sca} = \frac{k^4}{6\pi} |\alpha|^2 \quad (2)$$

where k is the wavevector of the incident light.

Silver nanoparticles were deposited directly on top of the silicon layer in SOI photodetector experiments. The above analysis shows that the plasmon frequency of a silver nanoparticle is red-shifted and its scattering cross section has increased nearly $(150)^2$ times for a given frequency when it is placed on the silicon layer. This analysis was for a single nanoparticle and the actual experimental films have particle size distributions that broaden these resonances.

A metallic nanoparticle in a homogeneous medium scatters light uniformly in all directions. When it is placed at the interface of two dielectric materials, it will scatter most of the incident field into the material with higher refractive index [17,18]. Soller *et al.* calculated the fraction of the light that is scattered by a dipole into different types of substrates [17]; 87% of the scattered light is directed into the top silicon layer when the dipole is on a SOI substrate. Thus, the enhancement in the normalized photoconductance spectra of SOI photodetectors is due to the increased scattering efficiency of the silver nanoparticles at longer wavelengths. We expect to observe similar enhancements in nc-Si:H solar cells at longer wavelengths when the annealed silver films are deposited directly on the top silicon layer instead of ITO layer.

CONCLUSIONS

We showed the results of annealed silver film deposition on top of nc-Si:H solar cells and SOI photodetectors. We have observed an overall reduction in the quantum efficiency of the solar cells with the addition of silver nanoparticles on their top ITO layers. This reduction was attributed to the extinction of the incident field by the large density of smaller diameter silver nanoparticles on the ITO layers. The normalized photoconductance spectra of SOI photodetectors was enhanced at longer wavelengths when the silver nanoparticles are prepared directly on their top silicon layers. Our analysis suggests that the plasmon frequency of the nanoparticles shifts into red and correlates well with the enhancement at longer wavelengths. The increase in the polarizability magnitude of the nanoparticles also improves their re-radiation efficiency leading to the observed enhancement of the photoconductance signal.

ACKNOWLEDGMENTS

This research has been partially supported by the U. S. Department of Energy through the Solar America Initiative (DE-FC36-07 GO 17053). Additional support was received from the Empire State Development Corporation through the Syracuse Center of Excellence in Environmental and Energy Systems.

APPENDIX

The polarizability α_0 of a spheroid embedded in a dielectric is given in the text of Bohren and Huffman as [16]:

$$\alpha_0 = V \frac{\varepsilon - \varepsilon_m}{\varepsilon_m + L(\varepsilon - \varepsilon_m)} \quad (3)$$

where ε is the dielectric constant of the material of the spheroid, ε_m is the dielectric constant of the embedding material, and V is the particle volume. The geometrical factor L for an oblate spheroid with semimajor axis r_{maj} and semiminor axis r_{min} is given by equation 5.34 in the reference:

$$L = \frac{g(e)}{2e^2} \left[\frac{\pi}{2} - \tan^{-1} g(e) \right] - \frac{g^2(e)}{2} \quad g(e) = \left(\frac{1 - e^2}{e^2} \right)^{1/2} \quad e^2 = 1 - \frac{(r_{min})^2}{(r_{maj})^2} \quad (4)$$

REFERENCES

1. E. Yablonovitch, *J. Opt. Soc. Am.* 72, 899 (1982).
2. H. R. Stuart and D. G. Hall, *Appl. Phys. Lett.* 69, 2327 (1996).
3. S. Pillai, K. R. Catchpole, T. Trupke and M. A. Green, *J. Appl. Phys.* 101, 093105 (2007).
4. F. J. Beck, S. Mokkaapati, A. Polman, and K. R. Catchpole, *Appl. Phys. Lett.* 96, 033113 (2010).
5. D. M. Schaadt, B. Feng, and E. T. Yu, *Appl. Phys. Lett.* 86, 063106 (2005).
6. J. Yang, B. Yan, G. Yue, S. Guha, *D. Mater. Res. Soc. Symp. Proc.* 1153, A13-02, (2009).
7. In previous studies, the surface was coated with a 30 nm lithium fluoride (LiF) spacer layer before the silver deposition [2,3]. We tested the effect of LiF layer and found that this layer had little effect; we did not use the LiF spacer layer for the measurements presented here.
8. B. Ozturk, H. Zhao, E. A. Schiff, B. Yan, J. Yang, S. Guha, unpublished.
9. B. T. Draine, P. J. Flatau, *J. Opt. Soc. Am. A* 11, 1491 (1994)
10. P. B. Johnson and R. W. Christy, *Phys. Rev. B* 6, 4370 (1972)
11. H. Mertens, J. Verhoeven, A. Polman, *Appl. Phys. Lett.*, Vol. 85, No. 8, 23 (2004)
12. B. Knoll, F. Keilmann, *Nature* 399, 134 (1999).
13. I. P. Protsenko and E. P. O'Reilly, *Phys. Rev. A* 74, 033815 (2006).
14. Y. S. Jung, *Thin Solid Films* 467, 36 (2004)
15. E. D. Palik, *Handbook of Optical Constants of Solids Vol.2* (AP,1991) and *Vol.3* (AP, 1998).
16. C. F. Bohren and D. R. Huffman, *Absorption and scattering of light by small particles* (Wiley-Interscience, New York, 1983)
17. B. J. Soller, H. R. Stuart, and D. G. Hall, *Opt. Lett.* 26, 1421 (2001).
18. J. Mertz, *J. Opt. Soc. Am. B* 17, 1906 (2000)